Journal of Vacuum Science and Technology A

RESEARCH ARTICLE | OCTOBER 10 2023

Stannane in extreme ultraviolet lithography and vacuum technology: Synthesis and characterization

Raquel Garza ; Nathan Bartlett ; Jameson Crouse ; Andrew Herschberg ; R. Mohan Sankaran ; Md. Amzad Hossain ; David N. Ruzic

J. Vac. Sci. Technol. A 41, 063209 (2023)
https://doi.org/10.1116/6.0002980

JVST A
Journal of Vacuum Science & Technology A
ARTICLE
pubs.aip.org/avs/jva

Stannane in extreme ultraviolet lithography and vacuum technology: Synthesis and characterization

Cite as: J. Vac. Sci. Technol. A **41**, 063209 (2023); doi: 10.1116/6.0002980
Submitted: 19 July 2023 · Accepted: 8 September 2023 ·
Published Online: 10 October 2023

View Online Export Citation CrossMark

Raquel Garza,[1,a)] Nathan Bartlett,[1,b)] Jameson Crouse,[1,c)] Andrew Herschberg,[1,d)] R. Mohan Sankaran,[1,e)] Md. Amzad Hossain,[1,2,f)] and David N. Ruzic[1,f)]

AFFILIATIONS

[1]Department of Nuclear, Plasma, and Radiological Engineering, Center for Plasma-Material Interactions, University of Illinois at Urbana-Champaign, Urbana, Illinois 61801
[2]Department of Electrical and Electronic Engineering, Jashore University of Science and Technology, Jashore 7408, Bangladesh

[a)]**Electronic mail:** raquelgza23@gmail.com
[b)]**Electronic mail:** nbb2@illinois.edu
[c)]**Electronic mail:** gcrouse3@illinois.edu
[d)]**Electronic mail:** ach3@illinois.edu
[e)]**Electronic mail:** rmohan@illinois.edu
[f)]**Authors to whom correspondence should be addressed:** mdamzadh@illinois.edu and druzic@illinois.edu

ABSTRACT

In extreme ultraviolet (EUV) lithography, tin droplets evaporate and subsequently coat various surfaces including the collector mirrors. To clean off the tin, a hydrogen plasma is often used, but as a result, an unstable by-product, stannane (SnH_4) is formed. The physicochemical characteristics of this gas, its formation in a plasma process, and its interaction with various materials have not been explored and understood completely. Here, the electron ionization mass spectrum of SnH_4 is presented. All ten natural abundance isotopes were observed experimentally for each fragment, i.e., Sn^+, SnH^+, $SnH_2{}^+$, and $SnH_3{}^+$. Density functional electronic structure theory was used to calculate the optimized ground state geometries of these gas phase species and their relative stabilities and helped explain the absence of $SnH_4{}^+$ in the observed signals. The density of the liquid, its cracking pattern, and the surface morphology of its deposits were examined. The surface of the deposited tin film resulting from the decomposition and subsequent oxidation was characterized by x-ray photoelectron spectroscopy. The main species found at the surface were metallic tin and tin (II) oxide (SnO). The detailed characterization of stannane should help correctly identify it in EUV lithographic processes and develop approaches in the future to mitigate its decomposition and redeposition on the collector mirrors or vacuum chamber walls.

I. INTRODUCTION

Extreme ultraviolet (EUV) lithography is the current cutting-edge optical lithography technique used in the semiconductor industry to fabricate integrated circuits. This technique employs radiation below ~50 nm wavelength to transfer patterns from a mask to a substrate, enabling smaller transistors and making chips more powerful, faster, and energy efficient.[1,2] EUV light is currently generated at 13.5 nm by irradiating tin (Sn) droplets with a carbon dioxide (CO_2) laser to produce a high charge state (+8 to +12) plasma.[3] However, an unintended consequence is that Sn evaporates and deposits on material surfaces, in particular, producing a detrimental impact on the collector mirror surfaces by decreasing their reflectivity.[4] One of the methods used for the removal of the tin coating on surfaces is a hydrogen plasma which produces stannane (SnH_4), a gas that can be evacuated by a pumping system.[5] As EUV systems become larger and larger, the flow requirements keep increasing and currently 100s of slm of hydrogen at 1 Torr are needed to deflect energetic Sn ions that come from the plasma. Concomitantly, concerns about what happens to SnH_4 in the plasma and on surfaces have become increasingly important.[6–10] Due to the unknown and unexplored reactivity of this gas, it is thus important to understand the properties of SnH_4.

In general, SnH_4 is a colorless inorganic and unstable gas, with a boiling and melting point of −52 and −146 °C, respectively. It decomposes slowly into Sn and $2H_2$ at room temperature.[11] The temperature characteristics make it a difficult gas to study. The first time SnH_4 is known to be synthesized was in 1924 by Paneth, who determined the vapor pressure and basic properties.[12–14] Extensive investigations have been published using organometallic derivatives of SnH_4 to obtain aromatic ketones and boronic acids.[15] Nevertheless, there are few publications about the synthesis and characterization of pure SnH_4.

Table I summarizes experimental details of previously reported approaches for SnH_4 synthesis. Overall, this compound has been mainly prepared by the reduction of tin (IV) chloride using sodium borohydride ($NaBH_4$) or lithium aluminum hydride ($LiAlH_4$) as reducing agents in solvents with different chemical natures. Schaeffer reported the highest yield using $SnCl_2$ and $NaBH_4$, which could also be considered the safest route due to the use of room atmosphere and temperature.[16] Some troubles related to oxidation issues and the need to dry the gas multiple times to obtain high purity have been observed using this method.[16] An air-free, atmospheric-pressure route using high boiling point organic solvents and a strong reducing agent ($LiAlH_4$) also allows the synthesis of this gas. This avoids the previously mentioned problems and is the technique used in this work.

In 1999, Girolami *et al.* published the experimental basics for the synthesis of inorganic and organometallic compounds, highlighting the vacuum line synthesis of germane.[17] Based on this synthesis, in 2018, Elg *et al.* synthesized SnH_4 gas and inserted it into a vacuum chamber with a Sn-coated quartz crystal microbalance to measure deposition at controllable temperatures.[10,18] They observed that at 5–6 Torr and temperatures of 20, 35, and 50 °C, no measurable deposition occurred, but at 110 °C, deposition occurred at a rate of 0.0044 Å/s. Additionally, they proved that the depositing material was Sn using x-ray photoelectron spectroscopy.

More direct characterization of SnH_4 has been carried out by mass spectrometry and the cracking pattern has been published. In 1961, Saalfeld and Svec reported the mass spectrum of SnH_4 considering the separated isotope ^{120}Sn. They obtained the ion fragmentation patterns for singly and doubly charged fragments. The relative intensities (%) for the fragments SnH_4, SnH_3, SnH_2, SnH, and Sn for singly charged ions were <0.1, 100, 53.6, 21.5, and 70.6, while for double charged ions were 0, 4.3, 5.7, 10.0, and <0.1, respectively.[19] In 1996, Aaserud and Lampe reported radiation-induced decomposition of SnH_4, resulting in the formation of H_2, Sn, as well as a very small amount of Sn_2H_6. The mass spectrum exhibited the highest intense peak (100%) at m/z 120, suggesting that stannylene was the principal intermediate in the reaction, which is analogous to the cases of silane and germane.[20]

Here, we report the measurement of the density of SnH_4 for the first time using the gravimetric method. Moreover, a mass spectrometry technique was used to identify the purity of the gas and to know which fragments are the most stable. To obtain real cracking pattern values, which have not been extensively reported, the spectrum was also calculated. This information has the potential to lead to an understanding of the properties of SnH_4 and in the future address its decomposition and re-deposition on the collector mirrors and other surfaces. The objectives of this work were to investigate the stannane synthesis using our operating conditions and to characterize our produced stannane using various diagnostic tools. In Sec. II, the experimental setup, physicochemical characteristics, and computational study are described in detail. The density of the liquid, cracking pattern, chemical surface analysis, surface morphology, and semiquantitative analysis of stannane are explained in Sec. III. Finally, in Sec. IV, the results obtained in this work are summarized.

II. METHODS

A. Stannane synthesis

Figure 1 shows the schematic diagram of the experimental setup used for stannane synthesis. The experiments were conducted in a fume hood. The anhydrous organic solvents were used without further purification. SnH_4 was synthesized following the methodology described by Elg *et al.*[18] with modifications. All glassware was cleaned and dried in an oven before starting the reaction and assembled according to the scheme shown in Fig. 1. The three

TABLE I. Summary of experimental details for previously reported approaches for the synthesis of SnH_4. The method reported in Elg *et al.* (Ref. 18) was used in this work.

Salt	Reducing agent	Solvent	Reactor temperature (°C)	Trap temperature (°C)	Yield	Vapor pressure (mm)	Reference
$SnCl_2$	$NaBH_4$	HCl/water	Room temperature	−23 −196	84%	39 (−105 °C) 198 (−78 °C)	16
$SnCl_4$	$LiAlH_4$	Ethyl glycol, diethyl ether	−196	−196	—		21
$SnCl_2$	KBH_4	HCl, KOH/water	Cold ice	−111	2.7%	17 (−111.6 °C)	22
$SnCl_4$	$LiAlH_4$	Diethyl ether	−70	−112 −196	30%		23
$SnCl_4$	$LiAlH_4$	1,2 dimethoxyethane dibutyl ether	−196	−96 −196	14%		18

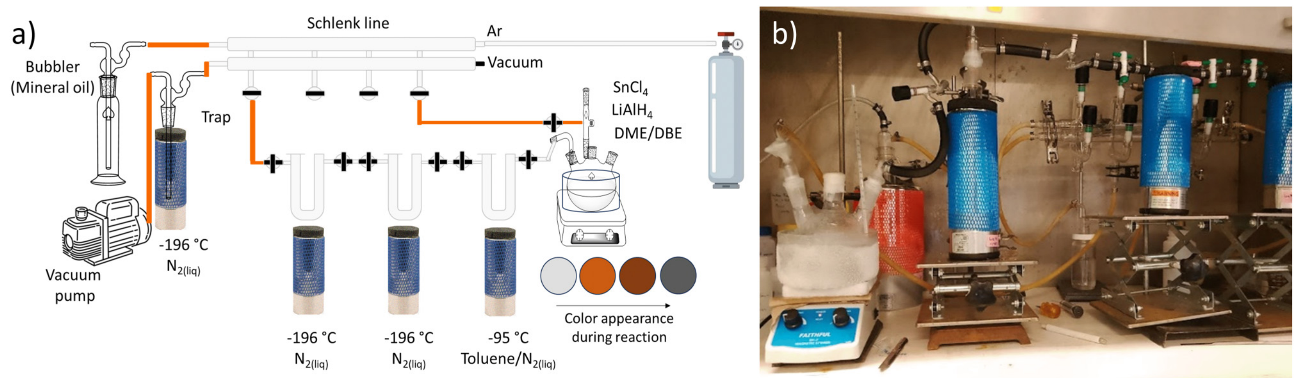

FIG. 1. (a) Schematic representation of the stannane synthesis using the Schlenk technique and (b) the real picture of the setup.

U-traps were isolated from the reactor and filled with argon gas and then evacuated three times using the Schlenk line to avoid any other gas or impurities. $LiAlH_4$ was placed into the reaction flask under argon flow to displace air from the atmosphere. Dibutyl ether and dimethoxyethane were added into the flask in equal volume proportion. After that, the flask was kept closed using a stopper, and the argon valve was also closed. The solution was stirred for 10 min. The three U-traps were immersed in the Dewars, where the inlet and outlet valves were kept closed. The first Dewar, which is close to the reaction flask, was kept at −95 °C using a slurry mixture of liquid nitrogen and toluene, with the aim of isolating the solvents. Two Dewars were placed at −196 °C using liquid nitrogen to trap the stannane liquid. Once the solution was stirred, the flask was placed in a bowl, in which liquid nitrogen was poured, with the aim of controlling the velocity of the reaction. After 15 min, $SnCl_4$ was introduced slowly using a borosilicate syringe, and all U-traps valves were opened except for the one placed before the Schlenk line. This valve was opened and closed every 5 min to remove any H_2 gas. The temperature of the flask was increased using a slurry of methanol and dry ice to reach −50 °C for 10 min and then until −30 °C for 1.5– 2.0h. The solution turned an orange/red color during the first 15 min and then, when the reaction started the black/gray color was observed. At this moment, the valve in the flask was opened partially to argon. This helps move the gaseous SnH_4 to the U-traps. The last valve was opened every 5 min to remove the hydrogen and argon gas from the traps. When the reaction was finished, each U-trap was isolated by closing all valves and storing the stannane liquid. The rubber tubing was made as short as possible. Some vacuum grease was added to the glass joints to form a seal. The glass joints were wrapped in parafilm multiple times to make a good seal. The argon gas flow was controlled by observing the bubbler. The temperature conditions were maintained strictly to avoid overpressure in the reaction flask.

B. Physicochemical characterization

Mass spectrometry was used to identify the gaseous ions produced by ionizing SnH_4 in crossed electric and magnetic fields based on their mass-charge ratios. The 70-VSE high-resolution spectrometer was operated using the electron-ion configuration. The gas was directly introduced into the ion source using narrow bore (0.25 mm) capillary columns. To verify the gas was SnH_4, decomposition was induced by heating the trap with a heat gun to potentially produce metallic tin. The semiquantitative composition of the samples was obtained by energy dispersive spectroscopy using a ThermoFisher Axia ChemiSEM microscope. X-ray photoelectron spectroscopy (XPS) was carried out to determine the surface composition as well as the chemical states of the film sample. Photoelectrons were generated with a non-monochromatic Mg Kα SPECS UXC-1000 source radiation (1253.68 eV) operating at 300 W and 15 keV. The photoelectrons were detected using a hemispherical analyzer with a pass energy of 20 eV. Corrections of the shift in the binding energy were made by fixing the energy of the C1 s peak from adventitious carbon in the films at 284.8 eV.

C. Computational study

The Sn—H structures were optimized and characterized with the PBE0 functional[24] in combination with the def2-TZVP basis set[25] using the ORCA 4.2.1 program.[26] The PBE0 functional was selected in this work because it provides good geometries and accurate energies for the main group elements. The results were visualized in CHEMCRAFT v1.8 software.[27]

III. RESULTS AND DISCUSSION

A. Density analysis

Density is a characteristic intensive property of a substance. The mass and volume must be determined, and the density depends on temperature and pressure. The density of liquid SnH_4 was obtained using a volumetric trap and an analytical balance. To minimize the temperature change when the trap was out of the Dewar, a flask with liquid nitrogen inside the balance was used to contain the trap. This allowed measuring the mass at approximately −196 °C and avoided fast evaporation of the liquid. Figure 2(a) shows the trap with liquid inside (the arrows indicate the volume level). Because SnH_4 starts to evaporate at −52 °C, to confirm that any excess liquid from the solvent used during the reaction was not present, the liquid was kept at room temperature. No liquid was found confirming that the liquid was pure SnH_4. The results of the density of various experiments are

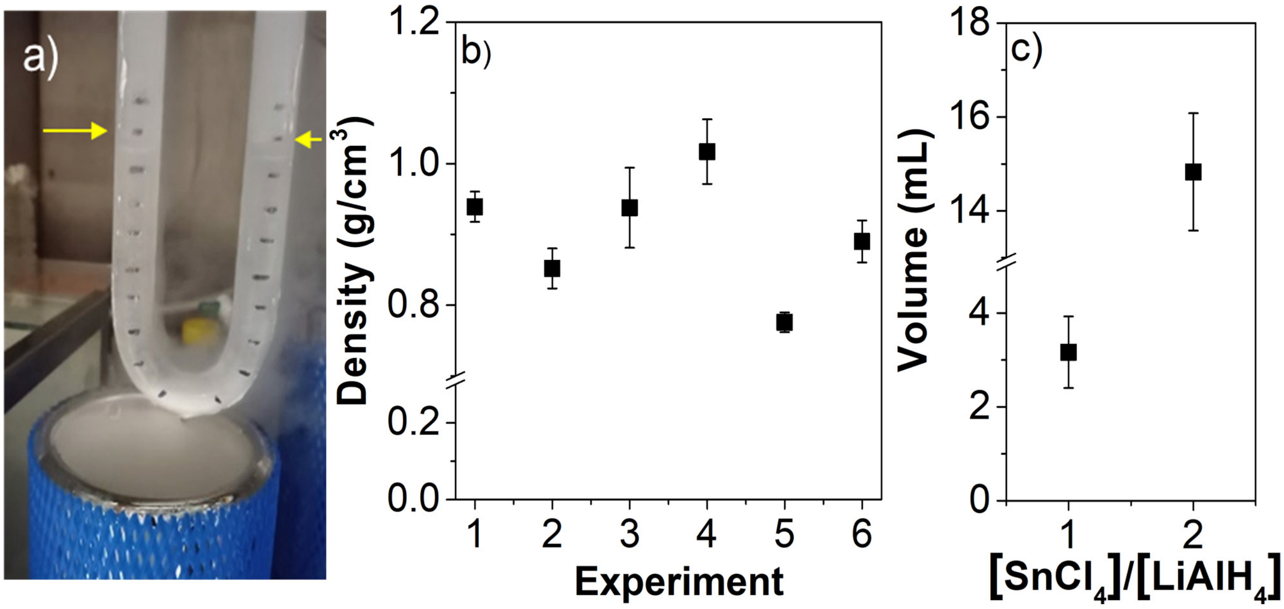

FIG. 2. (a) U-trap with SnH_4 liquid, (b) density values obtained at various experiments at −196 °C, and (c) volume of SnH_4 according to the ratio of $[SnCl_4]:[LiAlH_4]$.

shown in Fig. 2(b). The density of SnH_4 was found to range between 0.77 and 1.01 g/cm^3, for an average of 0.9 ± 0.10 g/cm^3. Additionally, the SnH_4 volume produced was increased by tuning the amount of $LiAlH_4$ used in the synthesis. This reagent is a fine powder that has low solubility in dimethoxymethane and dibutyl ether (0.53 mol/l). A small quantity of $LiAlH_4$ could be partially solubilized in the organic solvent and react uniformly. A high concentration of $LiAlH_4$ resulted in large agglomerates and the reaction did not completely occur. Figure 2(c) shows the volume of SnH_4 as a function of the ratio of concentrations of $SnCl_4$ to $LiAlH_4$. A ratio of 2:1 was found to maximize the SnH_4 volume trapped in our experiments [Fig. 2(c)].

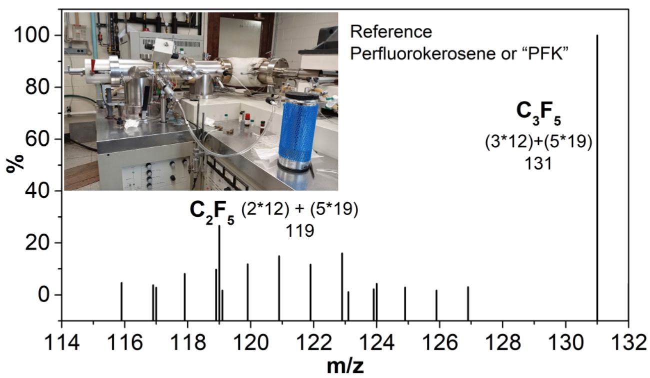

FIG. 3. Mass spectrometer coupled to U-trap (Dewar) and electron mass spectrum for stannane and perfluorokeresone (reference) compounds.

B. Cracking pattern analysis of stannane

Mass spectrometry through the high-resolution electron impact (EI) mode was performed to confirm the presence of SnH_4. The spectrometer was connected directly to the U-traps inlet and the U-traps were kept immersed in liquid nitrogen to avoid complete evaporation as shown in the inset of Fig. 3. To confirm that all the peaks observed in the spectrum are in good agreement with a known substance, a reference of perfluorokerosene was used. Two reference peaks located in the region of interest were observed. The peak's mass centered at 119 and 131 are attributed to C_2F_5 and C_3F_5, which agree with their mass expected.

Figure 4 shows the calculated and experimental mass spectra of different Sn—H species, and the resulting observed isotopic

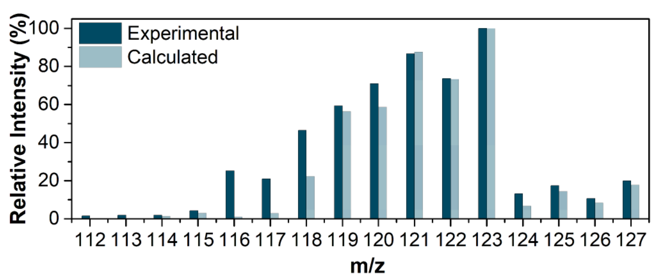

FIG. 4. Average positive EI mass spectrum of SnH_x^+ resulting from the ionization of SnH_4 obtained with an electron energy of 70 eV. The calculated spectra assume a 68 ± 3(%), 32 ± 2(%), 0.7 ± 0.02(%) cracking pattern to SnH_3, SnH_2, and SnH, respectively, and the known isotopic abundances.

TABLE II. Calculated and observed abundances of Sn—H species.

Mass	Calculated abundance (%)	Relative calculated abundance (%)	Measured relative abundance (%) Expt. 1	Measured relative abundance (%) Expt. 2
112	0.0	0.0	1.5	1.5
113	0.0	0.0	1.9	1.9
114	0.3	1.5	2	2.0
115	0.7	3.0	4.2	4.2
116	0.2	1.0	24.5	25.9
117	0.6	2.6	21.6	20.3
118	5.1	23.4	43.8	48.9
119	12.3	56.5	58.5	60.2
120	13.2	60.8	61.5	80.7
121	19.0	87.6	87.0	86.4
122	16.6	76.4	78.0	69.3
123	21.7	100.0	100.0	100.0
124	1.5	7.1	11.6	14.7
125	3.1	14.2	16.7	18.1
126	1.9	8.9	10.7	10.5
127	3.9	17.8	21.2	18.6

abundances are summarized in Table II. Tin has 10 stable isotopes, and it is important to consider all of them in the calculation to recognize the different peaks in a mass spectrum. Every single isotope according to its natural abundance contributes to the intensity of the peaks observed in the spectrum. SnH_4 has a molar mass of 122.71 g/mol (Sn: 118.71 g/mol and H: 1 g/mol); however, the most abundant Sn isotope is the one with a mass of 120. In this case, the most intense peak related to SnH_4 appeared around 124. While the ions Sn^+, SnH^+, $SnH_2{}^+$, and $SnH_3{}^+$ were all readily observed, the molecular $SnH_4{}^+$ ion was not observed. The limit of detection of the mass spectrometer was 1 ng and the reason $SnH_4{}^+$ was not detected is because of its low stability which leads to rapid decomposition before it reaches the detector. The following equations denote the processes involved in the fragmentation of SnH_4:

$$SnH_4 + e^- \rightarrow SnH_3^+ + H + 2e^-, \tag{1}$$

$$SnH_4 + 2e^- \rightarrow SnH_2^+ + 2H + 3e^-, \tag{2}$$

$$SnH_4 + 3e^- \rightarrow SnH^+ + 3H + 4e^-, \tag{3}$$

$$SnH_4 + 4e^- \rightarrow Sn^+ + 4H + 5e^-. \tag{4}$$

The most intense peak observed in the spectrum is located at 123, which is attributed to $SnH_3{}^+$. To determine the cracking pattern, simultaneous equations were written down for each isotope of Sn breaking into $SnH_3{}^+$, $SnH_2{}^+$, and SnH^+. The ratio of these three fragments was the variable to be determined. The observed mass peak was written as a sum of each isotope times the unknown cracking variables. This produces an overconstrained set of equations. The closest solution to fit all masses was the percentage fragments concentration of the species $SnH_3{}^+$, $SnH_2{}^+$, and SnH^+ of $68 \pm 3(\%)$, $32 \pm 2(\%)$, and $0.45 \pm 0.02(\%)$, respectively.

Table II shows the calculated and observed abundances of Sn—H species at various masses ranging from 112 to 127 obtained from two analyses. The average of both measurements is shown in Fig. 4.

Density functional theory (DFT) calculations were performed to assess the stability of the ionic fragments. Table III shows the calculated energies, bond lengths, bond angles, coordination, and multiplicities of various $SnH_X{}^+$ species. The results of the calculations are presented in Table III. The spin multiplicities of the odd species, SnH^+, and $SnH_3{}^+$ are singlets, while the even series result in doublet radical ions. The Sn—H bond lengths decrease from SnH^+ to $SnH_3{}^+$, indicating a stronger bond and greater stability. The largest even species, $SnH_4{}^+$, has three bond lengths of 1.687 Å except for one long bond of 2.239 Å, causing a very strained tetrahedron as is shown in Fig. 5. This suggests that $SnH_4{}^+$ will readily decompose to $SnH_3{}^+$ and contribute to the increased observed abundance of $SnH_3{}^+$ in the cracking pattern.

C. Chemical surface analysis of stannane

To further corroborate that the synthesized liquid was SnH_4, the U-trap was heated (>200 °C) to decompose the gas and produce a film, and the film was characterized by XPS. The film was found to mainly consist of carbon, oxygen, and tin. High-resolution spectra corresponding to Sn 3*d* and O 1*s* core energetic levels are shown in Fig. 6. The Sn 3*d* region shows two doublet peaks in 482.9 and 484.9 eV with a spin–orbit splitting of 8.41 eV attributed to the oxidation states Sn^0 and Sn^{2+},

TABLE III. Calculated energies, bond lengths, bond angles, coordination, and multiplicities of the $SnH_X{}^+$ species.

Species	Energy (hartree)	Gibbs free energy (kcal/mol)	Sn—H bond length (Å)	H—Sn—H bond angle (deg)	Coordination	Multiplicity
SnH^+	−214.606	− 134 665.7	1.760		Linear	Singlet
$SnH_2{}^+$	−215.157	− 135 011.124	1.724	120.13	Bent	Doublet
$SnH_3{}^+$	−215.765	− 135 392.873	1.686	120	Trigonal pyramid	Singlet
$SnH_4{}^+$	−216.281	− 135 716.553	1.687, 2.239	92.3, 119.9	Distorted tetrahedron	Doublet

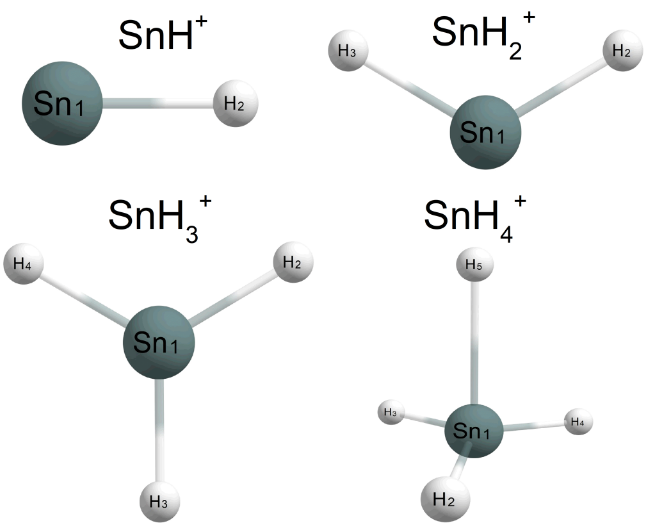

FIG. 5. Molecular structures for different SnH_x^+ computed at the PBE0/def2-TZVP level of theory.

respectively.[28] When a surface is exposed to the ambient, a monolayer of carbon is adsorbed in just milliseconds. The signal from this layer can be estimated by the Beer–Lambert equation to be ∼65% of the total signal. For this reason, the most intense peak of Sn should come from the SnO compound. Additionally, the oxygen spectrum consisted of four peaks. The peak located at lower binding energy (528.5 eV) was attributed to metal bonding, in this case, corresponding to SnO. The peak at 530.3 eV was assigned to O—Si bonding from the SiO_2 substrate.[29] The peaks centered at 531.7 and 533.1 eV correspond to O—C and O=C=O bonds, formed due to the adsorption of CO_2 from the atmosphere.[30]

TABLE IV. Semiquantitative composition obtained by EDS of the Sn surface.

Element	P1	P2	P3	P4	P5
C	10.5	12.8	10.9	18.5	14.8
Al	2.7	0.0	1.8	1.6	2.0
Cl	2.3	5.1	5.3	3.5	7.9
Sn	84.4	62.0	68.4	60.7	75.3
B	0.0	3.8	0.0	0.0	0.0
N	0.0	16.4	13.5	15.8	0.0

D. Semiquantitative analysis of stannane

The film deposited in the trap was peeled off for semiquantitative analysis by energy dispersive spectroscopy (EDS). Table IV shows the semiquantitative atomic concentration for five points along the sample, where the main elements found were C, Al, Cl, Sn, B, and N. Carbon, aluminum, and chlorine elements could come from the solvents (organics) and the metal precursors ($LiAlH_4$ and $SnCl_4$), respectively. On the other hand, the boron was attributed to the borosilicate glass used for the traps and other glass parts. Finally, nitrogen could come as an impurity from the gas that was used during heating to purge the setup and avoid the formation of SnO_2. A remarkable finding was that oxygen was not measured in the sample. This suggests that the oxygen found in XPS results was present only on the surface of the sample (7–10 nm) and not in the bulk of the material. Figure 7 shows a scanning electron microscopy (SEM) micrograph of a film after conversion. The image at higher magnification shows different pores at the surface which could be generated by the fast heating.

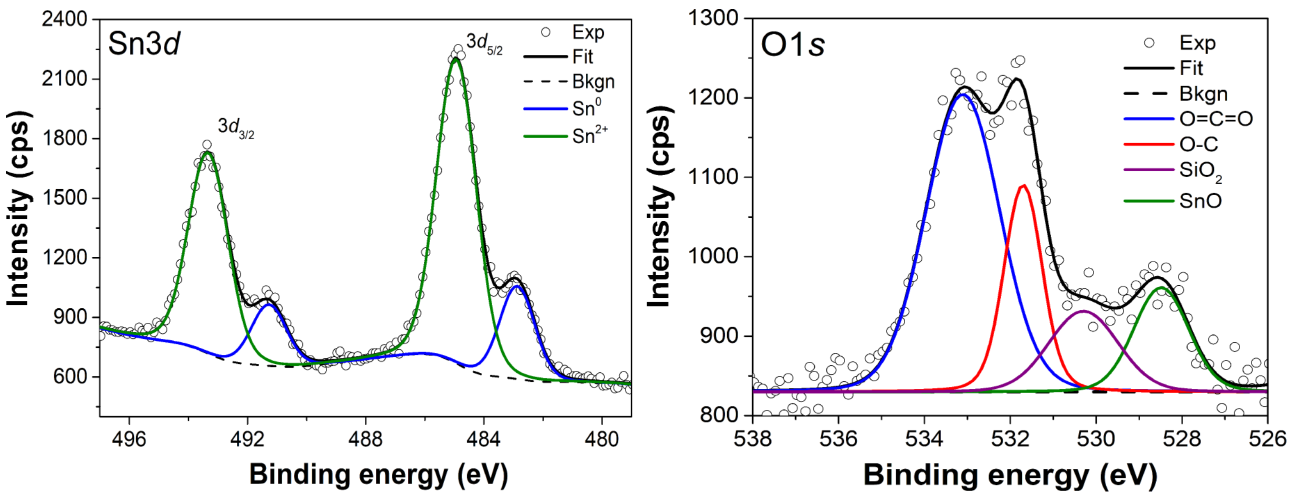

FIG. 6. XPS high-resolution spectra for Sn 3*d* and O 1*s* core energetic levels for Sn samples.

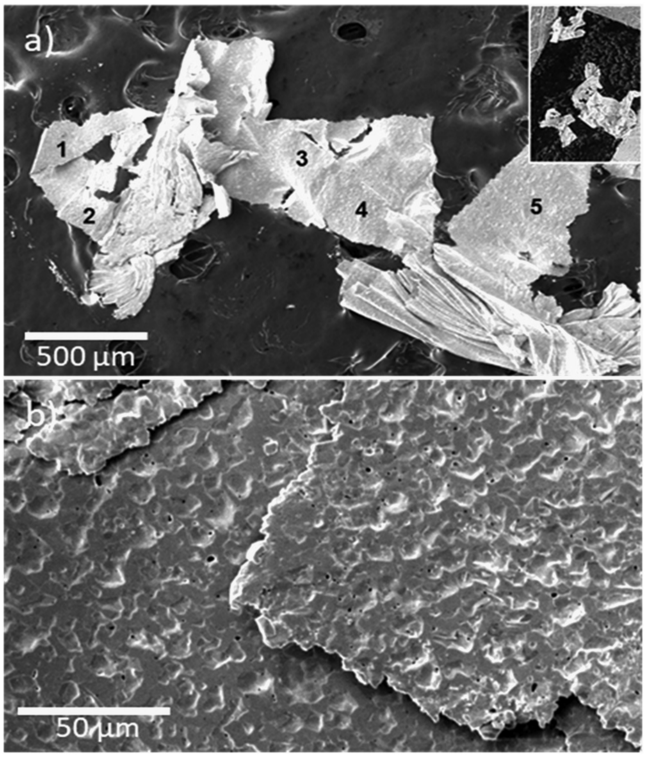

FIG. 7. SEM micrographs of Sn samples after conversion of SnH_4 to Sn. (a) At 500 μm scale, points 1, 2, 3, 4, 5 denote the locations of semiquantitative composition obtained by EDS of the Sn surface, and (b) at 50 μm scale, the picture is taken between points 1 and 2.

IV. CONCLUSIONS

The density of liquid stannane has been measured by a gravimetric method and the cracking pattern has been both measured and calculated by considering the abundance of the main peaks. These values are important for future uses and understanding of this compound. Remarkably, SnH_4^+ was not seen but its absence can be explained by looking at its binding structure using DFT. Future work will examine the decomposition of SnH_4 as a function of various temperatures and on different material surfaces.

ACKNOWLEDGMENTS

This research was financed by Advanced Semiconductor Materials Lithography (ASML) and EBARA Corporation. The authors are grateful for the characterization analysis which was carried out in part in the Materials Research Laboratory Central Research Facilities, University of Illinois.

AUTHOR DECLARATIONS

Conflict of Interest

The authors have no conflicts to disclose.

Author Contributions

Raquel Garza: Conceptualization (equal); Data curation (equal); Formal analysis (equal); Investigation (equal); Methodology (equal); Software (equal); Validation (equal); Writing – original draft (equal); Writing – review & editing (equal). **Nathan Bartlett:** Data curation (equal); Methodology (equal); Resources (equal). **Jameson Crouse:** Investigation (equal); Methodology (equal); Software (equal). **Andrew Herschberg:** Data curation (equal); Investigation (equal); Resources (equal); Software (equal). **R. Mohan Sankaran:** Conceptualization (equal); Investigation (equal); Methodology (equal); Supervision (equal); Visualization (equal). **Md. Amzad Hossain:** Formal analysis (equal); Investigation (equal); Project administration (equal); Supervision (equal); Writing – review & editing (equal). **David N. Ruzic:** Conceptualization (equal); Data curation (equal); Formal analysis (equal); Funding acquisition (equal); Investigation (equal); Methodology (equal); Project administration (equal); Resources (equal); Software (equal); Supervision (equal); Validation (equal); Visualization (equal); Writing – original draft (equal); Writing – review & editing (equal).

DATA AVAILABILITY

The data that support the findings of this study are available within the article.

REFERENCES

[1]C. Mbanaso and G. Denbeaux, "EUV lithography," in *Encyclopedia of Nanotechnology* edited by B. Bhushan (Springer, Dordrecht, 2012), pp. 797–803.
[2]B. Wu and A. Kumar, J. Vac. Sci. Technol. B **25**, 1743 (2007).
[3]M. Richardson, C.-S. Koay, K. Takenoshita, C. Keyser, and M. Al-Rabban, J. Vac. Sci. Technol. B **22**, 785 (2004).
[4]J. S. Kim, J. Choi, Y. J. Hong, and E. H. Choi, Plasma Chem. Plasma Process. **43**, 975 (2023).
[5]D. Qerimi, A. Herschberg, G. Panici, P. Hays, T. Pohlman, and D. N. Ruzic, J. Appl. Phys. **132**, 113302 (2022).
[6]D. N. Ruzic, *Electric Probes for Low Temperature Plasmas*, edited by W. Weed (American Vacuum Society, New York, 1994), pp. 1–93.
[7]F. F. Chen and J. P. Chang, *Lecture Notes on Principles of Plasma Processing* (Plenum, New York, 2002), pp. 1–208.
[8]M. A. Lieberman and A. J. Lichtenberg, *Principles of Plasma Discharges and Material Processing* (John Wiley & Sons, New York, 2005), pp. 1–748.
[9]D. Qerimi, G. Panici, A. Jain, D. Jacobson, and D. N. Ruzic, J. Vac. Sci. Technol. B **38**, 052601 (2020).
[10]D. T. Elg, G. A. Panici, S. Liu, G. Girolami, S. N. Srivastava, and D. N. Ruzic, Plasma Chem. Plasma Process. **38**, 223 (2018).
[11]N. N. Greenwood and A. Earnshaw, *Chemistry of the Elements* (Butterworth-Heinemann, Oxford, 1997), pp. 1–1283.
[12]F. Paneth and K. Fürth, Ber. Dtsch. Chem. Ges. A/B **52**, 2020 (1919).
[13]F. Paneth and E. Rabinowitsch, Ber. Dtsch. Chem. Ges. A/B **57**, 1877 (1924).
[14]F. Paneth, W. Haken, and E. Rabinowitsch, Ber. Dtsch. Chem. Ges. A/B **57**, 1891 (1924).
[15]R. A. Rossi, J. Organomet. Chem. **751**, 201 (2014).
[16]G. W. Schaeffer, S. M. Emilius, and O. S. F. Emilius, J. Am. Chem. Soc. **76**, 1203 (1954).
[17]G. S. Girolami, T. B. Rauchfuss, and R. J. Angelici, *Synthesis and Technique in Inorganic Chemistry*, edited by J. Stiefel (University Science Book, Sausalito, CA, 1999), pp. 65–77.

[18]D. T. Elg, G. A. Panici, S. Liu, G. Girolami, S. N. Srivastava, and D. N. Ruzic, Plasma Chem. Plasma Process. **38**, 917 (2018).
[19]F. E. Saalfeld and H. J. Svec, J. Inorg. Nucl. Chem. **18**, 98 (1961).
[20]D. J. Aaserud and F. W. Lampe, J. Phys. Chem. **100**, 10215 (1996).
[21]K. Tamaru, J. Phys. Chem. **60**, 610 (1956).
[22]W. L. Jolly, J. E. Drake, R. Rudolph, and T. Wartik, *Inorganic Synthesis*, edited by J. Kleinberg (McGraw-Hill Book Company, New York, 1963), Vol. 7, pp. 34–44.
[23]A. D. Norman, J. R. Webster, W. L. Jolly, R. A. Gorse, W. R. Bornhorst, and M. A. Ring, *Inorganic Synthesis*, edited by W. L. Jolly (McGraw-Hill Book Company, New York, 1968), Vol. 11, pp. 170–181.
[24]C. Adamo and V. Barone, J. Chem. Phys. **110**, 6158 (1999).
[25]F. Weigend and R. Ahlrichs, Phys. Chem. Chem. Phys. **7**, 3297 (2005).
[26]F. Neese, WIREs Comput. Mol. Sci. **8**, e1327 (2018).
[27]See https://www.chemcraftprog.com for "Chemcraft—Graphical Software for Visualization of Quantum Chemistry Computations."
[28]M. A. Stranick and A. Moskwa, Surf. Sci. Spectra **2**, 45 (1993).
[29]H. P. Ma, J. H. Yang, J. G. Yang, L. Y. Zhu, W. Huang, G. J. Yuan, J. J. Feng, T. C. Jen, and H. L. Lu, Nanomaterials **9**, 55 (2019).
[30]J. F. Moulder, W. F. Stickle, P. E. Sobol, and K. D. Bomben, *Handbook of X-Ray Photoelectron Spectroscopy*, edited by J. Chastain (Perkin-Elmer Corporation, Eden Prairie, MN, 1992), pp. 45–129.